

Direct observations of thermophoresis in microfluidic systems

Tetsuro Tsuji, Kosuke Kozai, Hideto Ishino, Satoyuki Kawano ✉

Graduate School of Engineering Science, Osaka University, Toyonaka 5608531, Japan

✉ E-mail: kawano@me.es.osaka-u.ac.jp

Published in Micro & Nano Letters; Received on 28th February 2017; Revised on 30th March 2017; Accepted on 5th April 2017

Particles transport driven by a temperature gradient in a solution is known as thermophoresis or Soret effect. The drift velocity \mathbf{v}_T of a particle is expressed as $\mathbf{v}_T = -D_T \nabla T$, where D_T is a thermophoretic mobility. Therefore, the thermophoretic mobility is a parameter to characterise the nature of thermophoresis, and the systematic measurement of D_T for various combinations of particles and solvents is necessary for its potential application. In the present work, we develop the microfluidic system called microgap Soret cell and show its validity by obtaining D_T for wide experimental conditions. It is shown that the microgap Soret cell can rapidly and directly obtain the thermophoretic mobility of a particle with the diameter of $O(1)\mu\text{m}$ by maintaining the large temperature gradient in the microfluidic system. Moreover, by using the microgap Soret cell, the temperature dependency of D_T is investigated for thermophoresis of polystyrene particles in solutions of sodium hydroxide, polyethylene glycol, and glycerol.

1. Introduction: Thermophoresis is the motion of nano/microparticles along the temperature gradient of surrounding fluids [1, 2] or gases [3, 4]. In particular, thermophoresis in fluids has attracted much attention due to its potential to measure the protein bindings [5] and biomolecule conformation [6]. Recently, thermophoresis of larger particles such as cells are also investigated using *Escherichia coli* [7], and the range of application is growing wider. It is expected that thermophoresis of biomolecules and cells can be applied to a new manipulation technology [8]. In such applications, we want to guide a target particle to a desired place. Thermophoresis toward the hot region is more preferable for this purpose since a local heating, which can be achieved by laser heating or Joule heating, is usually easier than a local cooling. The motion toward hotter regions is called negative thermophoresis, because in many cases the motion toward colder regions is observed. Therefore, it is important to investigate the conditions to realise negative thermophoresis. However, the thermophoresis of nano/microparticles arises as a result of the competition of various mechanisms [9], the theoretical understanding still lacks and the experimental studies are prevailing. In view of the development of thermophoretic manipulation technologies, the experimental setup for the precise investigation of negative thermophoresis with wide range of size is demanded.

Majority of the measurements of thermophoresis is based on the indirect detection of a steady concentration profile of target particles, formed as a result of thermophoretic transport of particles. To be more precise, the flux of the concentration c of the target particle in a non-uniform temperature field T counterbalances the flux induced by the thermophoretic velocity $\mathbf{v}_T \equiv -D_T \nabla T$ of the particle, i.e. $D\nabla c = c\mathbf{v}_T = -cD_T \nabla T$, where D_T is a thermophoretic mobility and D is a diffusion coefficient. This results in the exponential distribution $c \sim \exp(-S_T T)$ where $S_T = D_T/D$ is a Soret coefficient [10]. Most existing studies measure both c (or ∇c) and D to obtain D_T or measure only S_T . Thermal field-flow fractionation [11–13] and beam deflection (BD) [1, 2, 14–16], which are typical experimental setups, are both classified into this kind of measurement technique. The time scale τ for the establishment of the steady-state concentration is determined by a characteristic time $\tau \sim h^2/(\pi^2 D)$ [12, 14], where h is a length scale of the temperature variation. Therefore, the time scale of the experiment is dependent on D , which means it takes longer measurement time for larger particle. For instance, in the case of $h \sim 1\text{ mm}$ and the diameter d of the particle $d \sim 100\text{ nm}$, $\tau \sim 2 \times 10^4\text{ s} \sim 6\text{ h}$. Since the diffusion

coefficient linearly scales with d^{-1} using the Stokes–Einstein relation, the case of $d = 1\mu\text{m}$ takes 60 h and the accurate temperature control and a long experimental time are necessary. This is one of the reason of scarcity on the experiments using particles with a low diffusion coefficient, (e.g. $d \geq 1\mu\text{m}$), though we can find some [8, 11, 17]. In these studies, since the direction of the temperature gradient is orthogonal to that of gravity, it seems to be difficult to avoid the effect of thermal convection (see, e.g. [18]). In [6, 8, 10, 17], a laser heating is used to create large ∇T , and the resulting temperature profile may be complicated. Therefore, one has to pay attention to avoid non-thermophoretic effects such as thermal convection and optical trapping in these setups.

In the present Letter, we develop a simple experimental setup which achieves a fast evaluation on D_T . The setup is called *microgap Soret cell*, which is a Soret cell intended to produce a large temperature gradient while suppressing the unwanted effect by flows. The Soret cell is a typical and classical setting used in many existing studies (see, e.g. [19]), especially for the investigation of thermodiffusion of mixture [20, 21] and thermophoresis by BD technique (see, e.g. [14]). The microgap Soret cell is, as its name represents, the Soret cell with microgap, which enables to create large temperature gradient $|\nabla T| \geq 0.1\text{ K}/\mu\text{m}$ in a solution. Therefore, the thermophoretic velocity \mathbf{v}_T can exceed the velocity fluctuation by Brownian motion and be detectable by particle tracking technique. Moreover, by imposing the temperature gradient in the same direction as that of gravity, the inherent thermal convection in the existing study [11] can be suppressed. As a result of the improvements mentioned above, the measurement is free from non-thermophoretic contributions to the transport of particles and the running time can be decreased to tens of seconds. The microgap Soret cell is thus suitable for the systematic study of thermophoresis with small D , or equivalently, large diameter $d \geq 1\mu\text{m}$. This is a key improvement for the study of thermophoresis of particles with small D such as cells, which are recently explored as the new direction of application of thermophoresis [7]. In the present Letter, we measure the thermophoretic mobility of polystyrene (PS) particles with $d = 1\mu\text{m}$ in sodium hydroxide (NaOH) solutions and polyethylene glycol (PEG) solutions, which are expected to show the sign reversal of D_T depending on the concentration, according to Vigolo *et al.* [12] and Jiang *et al.* [22], respectively. Moreover, we investigate the thermophoresis of PS particles with $d = 3\mu\text{m}$ in glycerol solutions. Since the diameter of $d = 3\mu\text{m}$ is relatively large compared with a diameter around a couple of hundreds nanometres in existing studies and similar to the size of cells,

this diameter is an example of the thermophoresis of particles with a low diffusion coefficient that cannot be investigated by previous experimental setups. Therefore, we can demonstrate the applicability of the microgap Soret cell to such situations.

2. Experimental apparatus

2.1. Overview: We show the overview of our experimental setup in Fig. 1a. To visualise the thermophoresis of particles in the direction parallel to gravity, a zoom lens (VH-Z500R, Keyence, Japan) and a digital microscope (VHX, Keyence, Japan) are fixed horizontally as shown in Fig. 1. Accordingly, we introduce the Cartesian coordinates system $X = (X, Y, Z)$ such that the observation direction is the positive direction of Y and gravity is the negative direction of Z . The effect of the sedimentation of particles by gravity will be discussed in Section 3.1.

First, we describe the microgap Soret cell, which is indicated by bold-dashed square in Fig. 1a. Two copper (Cu) plates are aligned so that their distance h becomes a desired value. In the present Letter, we set $h \simeq 100 \mu\text{m}$. The alignment process is done carefully by observing the gap between two Cu plates through a microscope, and two microstages are used to align the distance between the Cu plates. Then, two acrylic plates sandwich the Cu plates in such a way that the gap is sealed. Two thermocouples are fixed to each Cu plate as shown schematically in Fig. 1a. The distance of thermocouples from the gap is 5 mm. The temperatures read by these thermocouples are defined as T'_1 and T'_2 .

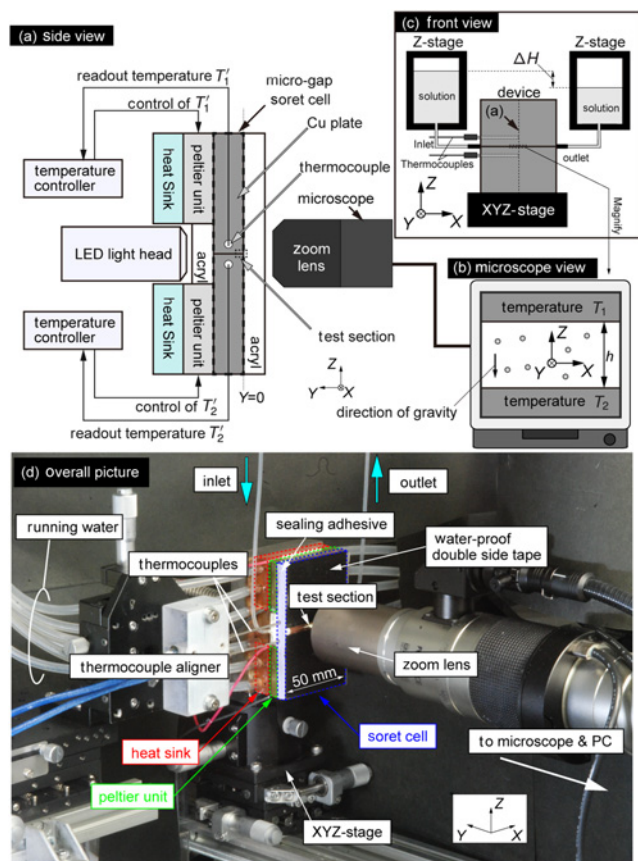


Fig. 1 Schematic view of the experimental system and the observation setup
a Side view
b Microscope view
c Front view
d Overall picture. Running water, sealing adhesive, water-proof double side tape, and thermocouple aligners are of secondary importance and omitted in panels (a)–(c). Test section is illuminated from the back by transmitted LED light

Next, we describe the temperature-control system in our experiment, which consists of Peltier units (CP60333, Cui Inc., USA), heat sink, and temperature controllers (OCE-TCR12075WL, Ohm Electric, Japan) in Fig. 1a. The temperature controllers and the Peltier units carry out the feedback control to keep T'_1 and T'_2 as desired. The temperature of the heat sink, $T_{\text{sink}} = 283 \pm 2 \text{K}$, is controlled by a water coolant using a recirculating chiller (CA-1115, Eyela, Japan). The piping of the water coolant is carefully isolated from the observation system since the interference of the pipes with the experimental setup can produce an undesired oscillation in the observation.

Transmitted light emitting diode (LED) light is used to visualise the particles as shown in Fig. 1a. The resulting microscope view is schematically described in Fig. 1b. The distance between two Cu plates is h and thus the plates consists the channel of height h . The temperatures of the upper wall and lower wall are, respectively, denoted by T_1 and T_2 . In general, the realisation of isothermal walls is difficult due to the heat escaping to the environment. Therefore, these values are not equal to the controlled values T'_1 and T'_2 . We measure the relation between the sets of (T_1, T_2) and the sets (T'_1, T'_2) in advance. Here, temperatures T_1 and T_2 are measured by another pair of thermocouples at the position 1.5 mm from the gap.

The flow control in the channel is achieved by the control of the water head difference ΔH between two reservoirs by electrical actuated Z-stages with $1 \mu\text{m}$ precision as shown in Fig. 1c. Note that Fig. 1b is the magnified figure of Fig. 1c near the channel. The whole device is mounted on the XYZ-stages.

2.2. Procedure: We summarise the experimental procedure as follows:

- (i) The reservoirs and the fluid channel are filled with the sample solution. Owing to the microgap of the present setup, it is hard to avoid having air bubbles in the channel, and their effect to the result cannot be ignored. Therefore, in order to evacuate air bubbles from the whole device, we deaerate the whole device and the reservoirs in a vacuum chamber.
- (ii) The temperatures of T'_1 and T'_2 are set to some desired values by using the temperature controllers. It takes 3 min for Cu plates to reach a steady state. Then, the steady temperature distribution of the solution is rapidly established since the thermal diffusivity of water, $\alpha_{\text{water}} = 0.143 \times 10^{-6} \text{m}^2/\text{s}$ at 300 K, indicates that the time scale for the temperature variation of water in $h \simeq 100 \mu\text{m}$ channel is $\tau_{\text{water}} \sim 0.1 \text{s}$. The observation duration is more than 20 s and large enough compared with τ_{water} . Therefore, the temperature of the solution, T_{sol} , is the linear function of Z and time independent

$$T_{\text{sol}}(Z) = T_m + \frac{\Delta T}{h}Z, \quad (1)$$

$$T_m \equiv \frac{T_1 + T_2}{2}, \text{ and } \Delta T = T_1 - T_2$$

where $Z = 0$ is defined at the centre of the channel.

- (iii) During the above procedures, the thermophoresis of particles takes place in a time-dependent manner, and the non-uniform particle distribution in the Z -direction is already established while we wait for the formation of steady temperature of Cu plates. Since we try to evaluate the thermophoresis by observing the particle velocity, it is better to have a uniform particle distribution at the beginning of video recordings. Therefore, using the water head difference between the two reservoirs, we induce the flow inside the fluid device in order to have the uniform distribution of particles. Note that

the temperature distribution T_{sol} of the solution (1) is kept established because of the small gap h and fast relaxation time $\tau_{\text{water}} \simeq 0.1$ s.

- (iv) Given the above situation, the motion of the particles under the temperature field [(1)] is recorded using the microscope with 1 fps for 20 s. Snapshots of 20 frames are used in particle tracking analysis. The duration more than 20 s is not favoured, since all the particles may come and stay near the Cu wall due to thermophoresis over this duration. This situation will be demonstrated in the snapshots of Section 3.1, where recording time is chosen to be 60 s. The particle tracking cannot be applied to such a situation.

Since we have temperature variation in the fluid, thermal convection may occur. To avoid thermal convection, the temperature of lower Cu plate is set to colder in most cases. However, in order to demonstrate that the thermophoresis can lift the particles against the gravity, we will show in Fig. 2 the case with the lower Cu plate heated. In the small gap of width h , the Rayleigh number, Ra , is estimated as

$$Ra = \beta g |\Delta T| h^3 / (\nu \alpha_{\text{water}}) \simeq 1, \quad \text{for } h = 100 \mu\text{m} \quad (2)$$

where $\beta = 3.0 \times 10^{-4} \text{K}^{-1}$ is the thermal-expansion coefficient, $g = 9.8 \text{m/s}^2$ is gravity acceleration, $\nu = 8.6 \times 10^{-7} \text{m}^2/\text{s}$ is the kinematic viscosity, and these numeric values are those for water at 300 K. It is theoretically predicted that the thermal convection, so-called Rayleigh–Bénard convection, occurs if a fluid contained in a gap of width h is heated from below and Ra is larger than its critical value [23] $Ra^c \simeq 1.7 \times 10^3$. In the present Letter, we obtain $Ra \simeq 0.5 \ll Ra^c$ by inserting $\Delta T = 20$ K to (2). Thus, it excludes the possibility of the convection in the gap.

3. Measurement results

3.1. Validation and accuracy: First, we show the time development of the particle motion. Fig. 2 shows the snapshots of the obtained video in the experiment at time $t = 0$ s, 10 s, ..., 60 s, where $h = 100 \mu\text{m}$. We use the dilute dispersion 10^{-3} wt% of PS particles of diameter $d = 1 \mu\text{m}$ (Estapor[®], Merck, USA) dispersed in a deionised water. The mass density of the PS particle is $\rho_{\text{PS}} = 1.05 \times 10^3 \text{kg/m}^3$. Since the dispersion is dilute, the density of the solution is the same as that of a solvent, i.e. $\rho_{\text{sol}} = 1 \times 10^3 \text{kg/m}^3$. The temperatures are set to $T_1 = 303.4$ K and $T_2 = 317.6$ K in Fig. 2, i.e. we have the temperature difference $\Delta T = -14.2$ K. Here and in what follows, the observation plane is $Y = 0.3$ mm, where $Y = 0$ mm indicates the surface of the Cu plates (see, Fig. 1a). It is seen that a region without particles grows near the hotter plate as time goes on. The arrow in Fig. 2 shows an example of the particle tracking, and indicates the particle migration toward the colder region. It can be

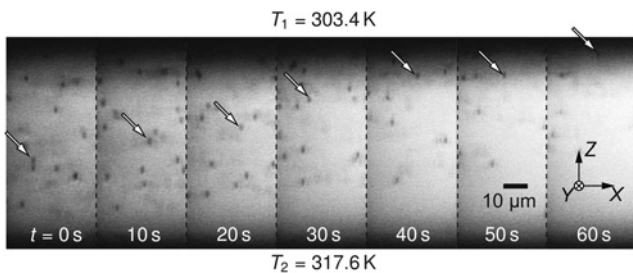


Fig. 2 Snapshots of the PS dispersion in the channel for the case of $T_1 = 303.4$ K and $T_2 = 317.6$ K. The arrow indicates an example of the particle tracking

roughly estimated from this figure that the Z-component of particle velocity V_Z is of the order of $\sim 1 \mu\text{m/s}$.

The probability distribution f to find a particle with the Z-component of the velocity V_Z is constructed from the result of particle tracking. We can obtain the averaged velocity \bar{V}_Z as the expectation value of f and its standard deviation σ of V_Z . Then, thermophoretic mobility D_T can be deduced from the equation

$$\bar{V}_Z = -D_T \frac{\partial T}{\partial Z} \simeq -D_T \frac{\Delta T}{h} \quad (3)$$

since the effect of thermal convection is negligible, thanks to the microgap developed in the present Letter.

Symbols in Fig. 3a show the result of particle tracking at $\Delta T = 13.5$ K with $T_m = 297$ K (white) and 310 K (green). The solid curves are the normalised Gaussian functions characterised by the mean value \bar{V}_Z and the standard deviation σ . It is seen that the experimental plots are well fitted by the Gaussian functions. The averaged velocity \bar{V}_Z is slightly below zero; however, the absolute value is smaller than σ . That is, the particles exhibit a Brownian motion but move toward the colder side (i.e. $\bar{V}_Z < 0$) on average. Moreover, one notes that the $|\bar{V}_Z|$ is larger in the case of $T_m = 310$ K. For various values of ΔT , \bar{V}_Z is plotted in Fig. 3b in the cases of $T_m = 297$ K (white), 302 K (red), 306 K (blue), and 310 K (green), where solid curves are the linear fit to the experimental plots. For all T_m , it is common that the increase of ΔT leads to the decrease of \bar{V}_Z . This trend corresponds to (3) with positive D_T . Therefore, Fig. 3b indicates that D_T is larger for larger T_m . The values of D_T will be given in Section 4.

Here, we give some comments on the diffusion coefficient obtained from the probability density f . The time scale of the observation is much longer than the relaxation time of the PS beads, thereby the mean-square-displacement (MSD) of the particle is related to D as $\text{MSD} = 2D\Delta t$ in the one-dimensional case, where Δt is the inverse of the frame rate. In the present Letter, $\Delta t = 1$ s results in $\sigma = \text{MSD}$, and D in the experiment, D_{exp} , can be obtained as $D_{\text{exp}} = \sigma^2/2$. On the other hand, the Stokes–Einstein relation gives the diffusion coefficient D_{theory} as $D_{\text{theory}} = k_B T / (3\pi\eta d)$, where k_B is the Boltzmann constant, T is the temperature of the solution and $T = T_m$ in our case, η is the viscosity of the solution. Here, the averaged value of $|D_{\text{theory}} - D_{\text{exp}}|/D_{\text{theory}} = 6.8 \times 10^{-2}$ is obtained from the data as shown in Fig. 3b. The agreement between the theory and the experiment is satisfactory and the method of analysis is validated.

We also note that the sedimentation of the PS particle is negligibly small, which can be seen from the data at $\Delta T \simeq 0$ K in

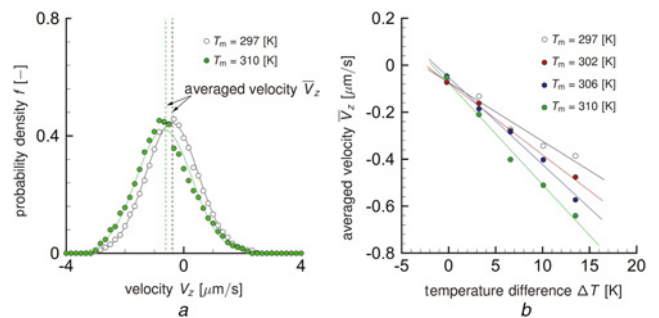


Fig. 3 Experimental results for PS particle of the diameter $1 \mu\text{m}$ in a deionised water

a Probability density f versus the Z-component of the particle velocity V_Z for the cases of $T_m = 297$ K (white) and 310 K (green) at $\Delta T = 13.5$ K
b Relation (3) for $T_m = 297$ K (white), 302 K (red), 306 K (blue), and 310 K (green)

Fig. 3b. The Stokes drag gives the sedimentation speed

$$v_s = d^2 g (\rho_{PS} - \rho_{sol}) (18\eta)^{-1} \quad (4)$$

where $\rho_{PS} = 1.05 \times 10^3 \text{ kg/m}^3$ is the mass density of the PS particle, $\rho_{sol} = 1.00 \times 10^3 \text{ kg/m}^3$ is the mass density of water, and $g = 9.8 \text{ m/s}^2$ is the acceleration of gravity. The averaged values of v_s as shown in Fig. 3b and the values by (4) are, respectively, 6×10^{-2} and $3 \times 10^{-2} \text{ } \mu\text{m/s}$. This difference is the indication of error in the particle tracking, and we conclude that the error is small compared with the velocities observed at larger ΔT .

3.2. Negative thermophoresis: The added electrolytes affect thermophoresis, and the sign of D_T can be controlled by the choice of the concentration. Following the existing studies [12, 13, 16], the experiments with the addition of NaOH is carried out for the concentration of NaOH $C_{NaOH} = 0, 2.5 \times 10^{-2}, 5.0 \times 10^{-2}, 7.5 \times 10^{-2},$ and $1.0 \times 10^{-1} \text{ mol/l}$. Here, the same data as Section 3.1 is used in the case of $C_{NaOH} = 0 \text{ mol/l}$ for a reference. In Fig. 4a, the probability densities for $0 \times 10^{-2} \text{ mol/l}$ (white), $2.5 \times 10^{-2} \text{ mol/l}$ (red), and $1.0 \times 10^{-1} \text{ mol/l}$ (magenta) are shown. As C_{NaOH} increases, the probability density shifts to the direction of positive V_Z , and the averaged velocity toward the hot region is obtained. The control of the direction by the adding NaOH has the possibility of the development of new manipulation technologies of particles. For $T_m = 310 \text{ K}$ and various ΔT , \bar{V}_Z is plotted in Fig. 4b in the cases of $2.5 \times 10^{-2} \text{ mol/l}$ (red), $5.0 \times 10^{-2} \text{ mol/l}$ (blue), $7.5 \times 10^{-2} \text{ mol/l}$ (green), and $1.0 \times 10^{-1} \text{ mol/l}$ (magenta). It is seen that, as ΔT increases, the \bar{V}_Z decreases for $C_{NaOH} = 2.5 \times 10^{-2} \text{ mol/l}$ and $C_{NaOH} = 0 \text{ mol/l}$, whereas \bar{V}_Z increases for other values of C_{NaOH} . The linear relation (3) holds for all cases and the increase of ΔT leads to the increase of $|\bar{V}_Z|$.

The addition of polymer is also proposed as the way to control thermophoresis by a laser irradiation [6, 22]. We use the PEG (PEG6000, Wako) as the polymer, and investigate the effect of the concentration C_{PEG} up to $C_{PEG} = 10 \text{ wt}\%$. In Fig. 5a, the probability densities f for $0 \text{ wt}\%$ (white), $6 \text{ wt}\%$ (magenta), and $10 \text{ wt}\%$ (dark purple) are shown. The apparent effect of the additive PEG on f is the smaller standard deviation, which is attributed to the increase of viscosity. In addition, \bar{V}_Z becomes small in magnitude for non-zero C_{PEG} , and the positive \bar{V}_Z is obtained at $\bar{V}_Z = 10 \text{ wt}\%$. For the case of $T_m = 310 \text{ K}$, \bar{V}_Z is plotted in Fig. 5b for various ΔT . The results are obtained for $0 \text{ wt}\%$ (white, see Section 3.1), $2 \text{ wt}\%$ (red), $3 \text{ wt}\%$ (blue), $4 \text{ wt}\%$ (green), $6 \text{ wt}\%$ (magenta), $8 \text{ wt}\%$ (light purple), and $10 \text{ wt}\%$ (dark purple). As in the case of Section 3.2, the increase of C_{PEG} up to $C_{PEG} = 10 \text{ wt}\%$ leads to

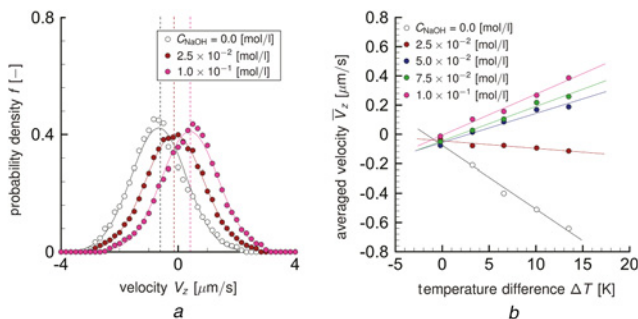


Fig. 4 Experimental results for PS particle of the diameter $1 \text{ } \mu\text{m}$ in a NaOH solution of various concentration C_{NaOH} and $T_m = 310 \text{ K}$
a Probability density f versus the Z -component of the particle velocity V_Z for the cases of $C_{NaOH} = 0 \text{ mol/l}$ (white), 0.025 mol/l (red), and 0.1 mol/l (magenta) at $\Delta T = 13.5 \text{ K}$
b Relation (3) for $C_{NaOH} = 0 \text{ mol/l}$ (white), 0.025 mol/l (red), 0.05 mol/l (blue), 0.075 mol/l (green), and 0.1 mol/l (magenta)

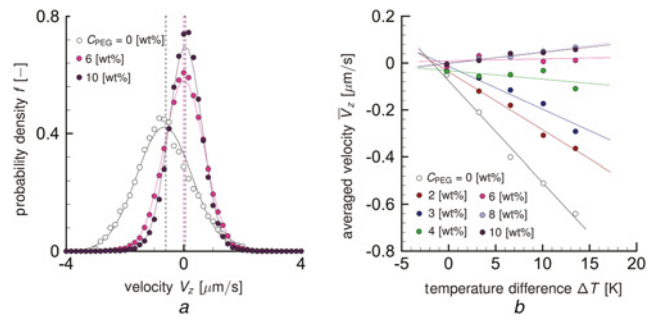


Fig. 5 Experimental results for PS particle of the diameter $1 \text{ } \mu\text{m}$ in a PEG solution of various concentrations C_{PEG} and $T_m = 310 \text{ K}$
a Probability density f versus the Z -component of the particle velocity V_Z for the cases of $C_{PEG} = 0 \text{ wt}\%$ (white), $6 \text{ wt}\%$ (magenta), and $10 \text{ wt}\%$ (dark purple) at $\Delta T = 13.5 \text{ K}$
b Relation (3) for $C_{PEG} = 0 \text{ wt}\%$ (white), $2 \text{ wt}\%$ (red), $3 \text{ wt}\%$ (blue), $4 \text{ wt}\%$ (green), $6 \text{ wt}\%$ (magenta), $8 \text{ wt}\%$ (light purple), and $10 \text{ wt}\%$ (dark purple)

the reversed trend of \bar{V}_Z against ΔT . To be more precise, at $C_{PEG} = 6 \text{ wt}\%$ or larger, the PS particles move toward the hot region. The linear relation (3) seems to hold for smaller $C_{PEG} \leq 3 \text{ wt}\%$; however, the plots are rather scattered for larger $C_{PEG} \geq 4 \text{ wt}\%$. We have confirmed that the similar plots corresponding to Fig. 5b are obtained for different values of T_m , though they are not shown. The thermophoresis toward the hot region in PEG solution without laser irradiation is obtained for the first time. Since the laser irradiation restricts the range of application, the sign reversal using PEG in such a simple channel, together with that observed in the NaOH solution, is expected to extend the possible application of thermophoresis.

3.3. Particle diameter dependence of $O(1) \text{ } \mu\text{m}$: Investigation on particles larger than $O(1) \text{ } \mu\text{m}$ will be useful in biological application. To investigate the thermophoretic behaviour of PS particles with a larger diameter in the present experimental setup, the use of a solution with a density close to that of PS is preferable. This is due to the fact that the sedimentation speed (4) is a quadratic function of d , and thus v_s may become comparable with the speed of thermophoresis. Therefore, we reduce the effect of sedimentation by using a glycerol solution prepared so that the mass density of the solution is close to that of PS.

The results of particle tracking for the cases with $d = 1$ and $3 \text{ } \mu\text{m}$ in a glycerol solution of a concentration $C_{Gly} = 20.4 \text{ wt}\%$ are shown in Fig. 6a. First, let us compare the cases of

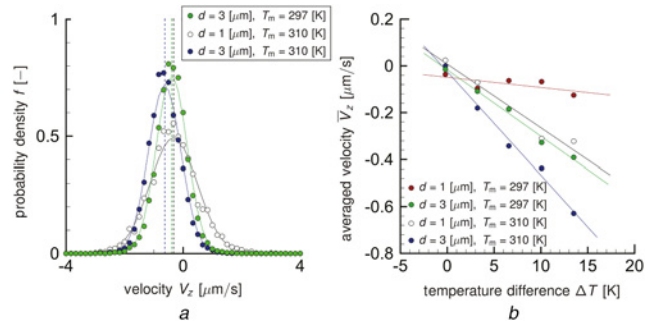


Fig. 6 Experimental results for PS particle of the diameter 1 and $3 \text{ } \mu\text{m}$ in a glycerol solution of $20.4 \text{ wt}\%$
a Probability density f versus the Z -component of the particle velocity V_Z for the cases of $d = 3 \text{ } \mu\text{m}$ and $T_m = 297 \text{ K}$ (green), $d = 1 \text{ } \mu\text{m}$ and $T_m = 310 \text{ K}$ (white), and $d = 3 \text{ } \mu\text{m}$ and $T_m = 310 \text{ K}$ (blue) at $\Delta T = 13.5 \text{ K}$
b Relation (3) for $d = 1 \text{ } \mu\text{m}$ and $T_m = 297 \text{ K}$ (red), $d = 3 \text{ } \mu\text{m}$ and $T_m = 297 \text{ K}$ (green), $d = 1 \text{ } \mu\text{m}$ and $T_m = 310 \text{ K}$ (white), and $d = 3 \text{ } \mu\text{m}$ and $T_m = 310 \text{ K}$ (blue)

$T_m = 297$ K (green) and $T_m = 310$ K (blue) with $d = 3$ μm . It is seen that thermophoresis in the direction toward the colder side is observed, and the speed is higher for larger T_m . This trend is the same as Section 3.1. We then compare the results for $d = 1$ μm (white) and $d = 3$ μm (blue) at $T_m = 310$ K. The probability density for $d = 3$ μm is steeper, and \bar{V}_Z takes larger value than the case of $d = 1$ μm . Smaller standard deviation for $d = 3$ μm is due to the smaller diffusion coefficient. The averaged velocity \bar{V}_Z versus ΔT is shown in Fig. 6b for $d = 1$ μm , $T_m = 297$ K (red), $d = 3$ μm , $T_m = 297$ K (green), $d = 1$ μm , $T_m = 310$ K (white), and $d = 3$ μm , $T_m = 310$ K (blue). It is seen that the linear relation (3) also holds for the PS particles with $d = 3$. In the case of glycerol solution, the thermophoretic motion toward the hotter region, which is observed in NaOH and PEG solutions, does not occur within the present experimental conditions.

4. Discussion of thermophoretic mobility D_T : In this section, we summarise the results obtained in previous sections by comparing the T_m -dependence of D_T for various conditions. D_T is evaluated from (3) and the gradients of the linear fits in Figs. 3b–6b.

First, we describe the case of a deionised water in Fig. 7a, where the error bars indicate the residual from the fit. It seems that D_T is a linearly increasing function of T_m . The linear relation is also found in the existing study [24] for much smaller PS bead with diameter 30 nm. It is also pointed out that the sign reversal of D_T can occur as T_m decreases to around 277 K, where the density of the solution takes maximum. In other words, thermophoresis in water is related to thermal expansivity of the water [24]. To check the same is true for the present case with $d = 1$ μm , we extrapolate

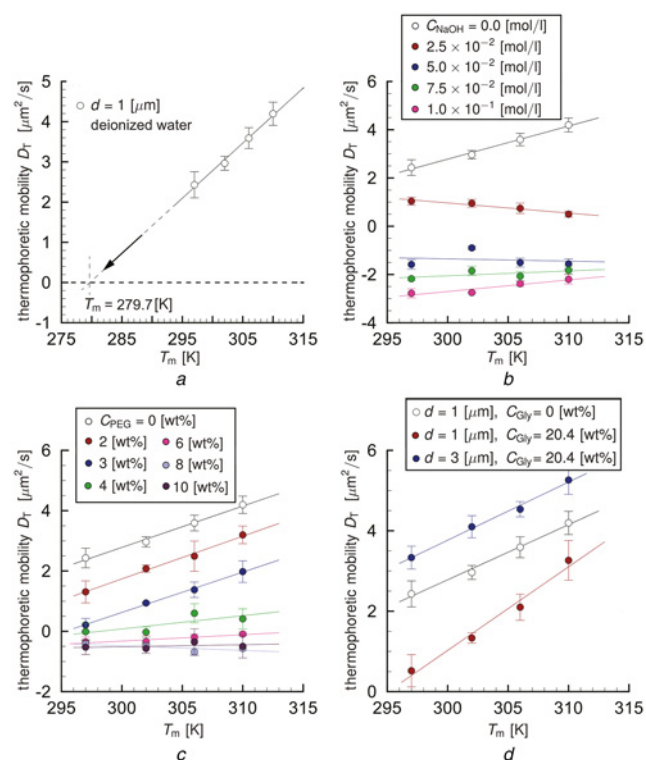


Fig. 7 Thermophoretic mobility D_T versus temperature $T_m = 297$ K, 302, 306, and 310 K for the experimental conditions investigated in the present Letter

a and b The cases of the NaOH solution: $C_{\text{NaOH}} = 0$ mol/l (white), 0.025 mol/l (red), 0.05 mol/l (blue), 0.075 mol/l (green), and 0.1 mol/l (magenta)

c Cases of the PEG solution: $C_{\text{PEG}} = 0$ wt% (white), 2 wt% (red), 3 wt% (blue), 4 wt% (green), 6 wt% (magenta), 8 wt% (light purple), and 10 wt% (dark purple)

d Cases of the glycerol solution: $d = 1$ μm , $C_{\text{Gly}} = 0$ wt% (white), $d = 1$ μm , $C_{\text{Gly}} = 20.4$ wt% (red), and $d = 3$ μm , $C_{\text{Gly}} = 20.4$ wt% (blue)

the result by a linear function as shown in Fig. 7a. In our case, the temperature for $D_T = 0$ is estimated as $T_m = 279.7$ K, which is slightly higher than the existing study [24]. Since it is the extrapolation, we only conclude that the agreement between [24] and the present result is qualitative. To carry out the experiment with lower T_m , it is necessary to put the whole experimental system in a temperature-controlled environment. This is the point to be improved in the future study.

Fig. 7b shows D_T for NaOH solutions discussed in Section 3.2. Obviously, the addition of NaOH triggers the drastic decrease of D_T . For $C_{\text{NaOH}} \geq 5 \times 10^{-2}$ mol/l, D_T becomes negative. The T_m -dependence is also suppressed for $C_{\text{NaOH}} > 0$ mol/l. This trend is also observed in [13], where smaller particles of diameter 215 nm and weaker solution is used. For $C_{\text{NaOH}} \geq 2.5 \times 10^{-2}$ mol/l, D_T seems to decrease as T_m increases, which is unusual behaviour. We think this may be due to an error arising from slow thermophoretic velocities for this particular condition. In fact, the thermophoretic velocity is the order of ~ 0.1 $\mu\text{m/s}$ (compare the red symbols in Fig. 4) and this is of the same order of the tracking error $\sim 3 \times 10^{-2}$ μm discussed below (4). The sign reversal and T_m -insensitive behaviour of D_T in NaOH solution suggests the different mechanism of thermophoresis from the one in the deionised water. The proposed mechanism is a so-called thermoelectricity induced by the temperature gradient in a solution [25]. Thermoelectricity have been discussed in surfactant solution or the dispersion of charged colloidal particles with nanometre scale [12, 13, 16]. It is explained in [16] that the OH^- ions are more likely to accumulate toward the colder side than Na^+ ions and the resulting inhomogeneous ion distribution generates a thermoelectric field, which drives the negatively charged PS beads to the hotter side. However, the C_{NaOH} -dependence is studied only for the thermophoresis of micelles of radius $\simeq 2.5$ nm in the existing study [16], whereas thermophoresis of PS beads for $C_{\text{NaOH}} = 0.1$ mol/l is investigated in [12]. The present Letter complements the C_{NaOH} -dependence on the thermophoresis of PS particle for various T_m , thanks to the systematic experimental setup for parameter study.

Fig. 7c is the summarised results of Section 3.2 for PEG solutions. As C_{PEG} increases, D_T decreases and becomes negative for $C_{\text{PEG}} \simeq 6$ wt% or more. It should be noted that the temperature dependency is also suppressed, and there seems no clear temperature dependence for $C_{\text{PEG}} = 8$ and 10 wt%. As in the case of NaOH solutions, the decrease and the insensitivity of D_T for increasing C_{PEG} is due to the different mechanisms of thermophoresis from the one in the deionised water. In the case of PEG, the mechanism is considered to be the diffusiophoresis [22] induced by a PEG concentration gradient. We obtain qualitatively the same result as [22]. However, the value of $C_{\text{PEG}}^{\text{critical}}$, such that $D_T = 0$, $C_{\text{PEG}}^{\text{critical}}$, is different. In [22], $C_{\text{PEG}}^{\text{critical}}$ is between $C_{\text{PEG}} = 1$ and 2 wt%. On the other hand, $C_{\text{PEG}}^{\text{critical}}$ seems to be between $C_{\text{PEG}} = 4$ and 6 wt% in this Letter. This may be attributed to the difference of geometries of heating. The laser irradiation at a spot is used in [22] as a heating method, and thus it produces a concentric concentration gradient of PEG, which enhances the motion of PS particle toward the spot. Our results for PEG solutions, together with those for NaOH solutions mentioned above, extend the results of existing studies to larger particle diameter range.

Finally, we show the results of Section 3.3 in Fig. 7d. Here, we do not have the sign reversal of D_T for all T_m investigated. The comparison between $d = 1$ μm , $C_{\text{Gly}} = 0$ wt%, and $d = 1$ μm , $C_{\text{Gly}} = 20.4$ wt% shows that the addition of glycerol decreases D_T . Note that the viscosity of glycerol $C_{\text{Gly}} = 20$ wt% is 1.33 times higher than a pure water [26]. The decrease may be partly attributed to the increase of viscosity (see the model in [27]) and partly attributed to the difference of interfacial tension between the PS particle and the solvent. To investigate this point in detail, we have to change viscosity of the solvent without changing the interfacial property. This is not straightforward, and will be

considered in a separate work. The comparison between $d = 1$ and $3 \mu\text{m}$ shows that D_T for $d = 3 \mu\text{m}$ is larger than that of $d = 1 \mu\text{m}$. This is not consistent with the existing study which shows the size-independent D_T for smaller PS particles ($d \leq 253 \text{ nm}$) in surfactant [15]. As stated in [27], the thermophoresis of colloid consists of diffusive contribution and hydrodynamic contribution, which originates from a Marangoni-type slip flow. The former is superior for the particles with relatively large diffusion coefficient such as those studied in [15], whereas the latter becomes significant for the particles with small diffusion coefficient as in the present Letter. Note that the latter contribution is proportional to the diameter [27]. In fact, according to the criteria suggested in (1) in [28], our experimental condition violates the assumption of a thermodynamic equilibrium and thus needs fluid-dynamic treatment [27]. Therefore, the increase of D_T for $d = 3 \mu\text{m}$ may not be explained by the theories or experiments for smaller colloids or biomolecules [15]. For further understanding of thermophoresis, systematic studies with larger diameters should be carried out, which will be our future work.

5. Concluding remarks: In the present Letter, we have established the experimental setup called the microgap Soret cell, which enables a rapid evaluation of thermophoretic mobility of particles. The advantage of the present setup is that we can directly observe the thermophoretic motion of particles with small diffusion coefficient, thanks to the large temperature gradient produced by the microgap. This enables us to obtain the thermophoretic mobility directly from the explicit relation $v_T = -D_T \nabla T$. The validity of the experiment is confirmed by comparing the present results with some existing studies. To be more precise, we have checked the temperature dependence of thermophoretic mobility, the sign reversal in NaOH solutions and PEG solutions. The qualitative and partly quantitative agreements are obtained.

6. Acknowledgments: The present study was supported by Japan Society for the Promotion of Science (JSPS) KAKENHI grant no. JP15K17973 for Young Scientists (B) and JSPS KAKENHI grant no. JP16H06504 in Scientific Research on Innovative Areas ‘Nano-Material Optical-Manipulation’.

7. References

- [1] Piazza R., Parola A.: ‘Thermophoresis in colloidal suspensions’, *J. Phys., Condens. Matter*, 2008, **20**, p. 153102
- [2] Piazza R.: ‘Thermophoresis: moving particles with thermal gradients’, *Soft Mat.*, 2008, **101**, p. 168301
- [3] Chapman S., Cowling T.G.: ‘The mathematical theory of non-uniform gases: an account of the kinetic theory of viscosity, thermal conduction and diffusion in gases’ (Cambridge University Press, Cambridge, 1970)
- [4] Sone Y.: ‘Molecular gas dynamics: theory, techniques, and applications’ (Birkhäuser, Boston, 2007)
- [5] Wienken C.J., Baaske P., Rothbauer U., *ET AL.*: ‘Protein-binding assays in biological liquids using microscale thermophoresis’, *Nat. Commun.*, 2010, **1**, p. 100
- [6] Maeda Y.T., Tlustyd T., Libchaber A.: ‘Effects of long DNA folding and small RNA stem-loop in thermophoresis’, *Proc. Natl. Acad. Sci. USA*, 2012, **109**, pp. 17972–17977
- [7] Chen J., Cong H., Loo F.-C., *ET AL.*: ‘Thermal gradient induced tweezers for the manipulation of particles and cells’, *Sci. Rep.*, 2016, **6**, p. 35814
- [8] Duhr S., Braun D.: ‘Why molecules move along a temperature gradient’, *Proc. Natl. Acad. Sci. USA*, 2006, **103**, pp. 19678–19682
- [9] Würger A.: ‘Thermal non-equilibrium transport in colloids’, *Rep. Prog. Phys.*, 2010, **73**, pp. 126601
- [10] Duhr S., Braun D.: ‘Thermophoretic depletion follows Boltzmann distribution’, *Phys. Rev. Lett.*, 2006, **96**, p. 16831
- [11] Regazzetti A., Hoyos M., Martin M.: ‘Experimental evidence of thermophoresis of non-Brownian particles in pure liquids and estimation of their thermophoretic mobility’, *J. Phys. Chem. B*, 2004, **108**, pp. 15285–15292
- [12] Vigolo D., Rusconi R., Stone H.A., *ET AL.*: ‘Thermophoresis: microfluidics characterization and separation’, *Soft Mat.*, 2010, **6**, pp. 3489–3493
- [13] Eslahian K.A., Majee A., Maskos M., *ET AL.*: ‘Specific salt effects on thermophoresis of charged colloids’, *Soft Mat.*, 2014, **10**, pp. 1931–1936
- [14] Piazza R.: ‘Thermal diffusion in ionic micellar solutions’, *Phil. Mag.*, 2003, **83**, pp. 2067–2085
- [15] Braibanti M., Vigolo D., Piazza R.: ‘Does thermophoretic mobility depend on particle size?’, *Phys. Rev. Lett.*, 2008, **100**, pp. 108303
- [16] Vigolo D., Buzzaccaro S., Piazza R.: ‘Thermophoresis and thermoelectricity in surfactant solutions’, *Langmuir*, 2010, **26**, pp. 7792–7801
- [17] Schermer R.T., Olson C.C., Coleman J.P., *ET AL.*: ‘Laser-induced thermophoresis of individual particles in a viscous liquid’, *Opt. Express*, 2011, **19**, pp. 10571–10586
- [18] Landau L.D., Lifshitz E.M.: ‘Fluid mechanics’ (Elsevier, 1987, 2nd edn.)
- [19] McNab G.S., Meisen A.: ‘Thermophoresis in liquids’, *J. Colloid Interface Sci.*, 1973, **44**, pp. 339–346
- [20] Kolodner P., Williams H., Moe C.: ‘Optical measurement of the Soret coefficient of ethanol/water solutions’, *J. Chem. Phys.*, 1988, **88**, pp. 6512–6524
- [21] Mialdun A., Shevtsova V.: ‘Temperature dependence of Soret and diffusion coefficients for toluene–cyclohexane mixture measured in convection-free environment’, *J. Chem. Phys.*, 2015, **143**, p. 224902
- [22] Jiang H.-R., Wada H., Yoshinaga N., *ET AL.*: ‘Manipulation of colloids by a nonequilibrium depletion force in a temperature gradient’, *Phys. Rev. Lett.*, 2009, **102**, p. 208301
- [23] Reid W.H., Harris D.L.: ‘Some further results on the Bénard problem’, *Phys. Fluids*, 1958, **1**, pp. 102–110
- [24] Iacopini S., Rusconi R., Piazza R.: ‘The ‘macromolecular tourist’: universal temperature dependence of thermal diffusion in aqueous colloidal suspensions’, *Eur. Phys. J. E*, 2006, **19**, pp. 59–67
- [25] Würger A.: ‘Transport in charged colloids driven by thermoelectricity’, *Phys. Rev. Lett.*, 2008, **101**, p. 108302
- [26] Segur J.B., Oberstar H.E.: ‘Viscosity of glycerol and its aqueous solutions’, *Ind. Eng. Chem.*, 1951, **43**, pp. 2117–2120
- [27] Würger A.: ‘Thermophoresis in colloidal suspensions driven by Marangoni forces’, *Phys. Rev. Lett.*, 2007, **98**, p. 138301
- [28] Weinert F.M., Braun D.: ‘Observation of slip flow in thermophoresis’, *Phys. Rev. Lett.*, 2008, **101**, p. 168301